

## Effect of slit-type barrier on characteristics of water-dominant debris flows: small-scale physical modeling

**Abstract** Slit-type barriers, one of open-type barriers, are widely used as active measures to mitigate potential risk and damage by debris flows, and those are designed and installed to reduce the flow energy by only passing relatively small debris. However, the mechanisms of slit-type barriers in reducing the debris flow velocity and debris volume remain poorly understood because of the lack of well-controlled and reliable physical modeling results. This study explored the influence of various arrangements of slit-type barriers, including P-type barriers in which each rectangular barrier was placed in parallel and V-type barriers where the barriers were placed in a V-shape, on characteristics of water-dominant debris flows via small-scale model experiments. The debris flow events were reproduced against the slit-type barriers, where the velocity reduction and trap ratio were monitored, varying the angle and shape of barrier arrangements. The velocity reduction and trap ratio appeared to increase as the angle of the barrier wall decreased because of the decreased opening ratio. The V-type barriers resulted in higher velocity reduction and trap ratio than the P-type, primarily because of the smaller effective opening ratio and the more backwater effect. In addition, as the debris contained more boulders, the extent of velocity reduction and debris trap became greater in all barrier types. Two types of opening ratios, the projected and effective opening ratios, were correlated to the interactions between debris and walls. The obtained results provide baseline data for the optimum design of slit-type barriers against debris flow and suggest that the slit-type barriers can effectively manage the risk of damage by debris flows.

**Keywords** Debris flow · Slit-type barrier · Opening ratio · Velocity reduction · Trap ratio · Physical modeling

### Introduction

A debris flow is a landslide that transports suspended loads and bedloads in mountain torrents with great fluidity (Evans 1982; Sharpe 1938; Swanson and Swanson 1976). Such flow carries debris that consists of various mixtures of large and coarse materials (boulders and driftwoods) and fines (silt and clay) (Iverson 1997; Nasmith and Mercer 1979), and the space between the solid debris is filled with water or slurry (Pierson 2005). This composition is mainly determined by the sediment characteristics of the basin where the debris flow occurs (Lister et al. 1984). The debris flow can cause severe damage to urban areas because it entrains material at the bottom of a steep channel, carrying a huge volume of debris at a high flow velocity (Hübl et al. 2009; Hung et al. 1984; Jakob et al. 2005). Debris flow barriers to reduce the debris flow velocity are widely used as active mitigation measures to prevent damage to urban areas (Zollinger 1985). There are two kinds of debris flow barriers: one is a closed-type barrier that is designed to trap all of the generated debris flow, and the other is an open-type barrier that intends to separate big debris, such as gravels, cobbles,

boulders, and driftwoods, from debris flows, reducing the flow energy. An open-type barrier is designed to intercept part of the flow and, more importantly, to control the peak discharge of the debris flows by only passing relatively small debris that is expected to cause minimal damage (Takahashi 2014). A slit-type barrier, one of the frequently installed types of open-type barriers, is similar to the closed-type barrier, but it has multiple vertical slits at the barrier wall, where the debris larger than the opening size is trapped and deposited. Accordingly, the majority of previous studies have examined the effect of slit size or geometry on trap performance, mostly correlating the reduction of the debris volume and the density to the ratio of the slit spacing to the maximum diameter of the debris (i.e.,  $b/d_{\max}$  ratio) or to the ratio of the slit spacing to the channel width (i.e.,  $\sum b/B$  ratio) (Ikeya and Uehara 1980; Watanabe et al. 1980; Wenbing and Guoqiang 2006). The small discharge capacity of this particular class of slit-type barriers causes a significant backwater effect, where a part of the debris flow that hits the barrier wall bounces backward and blocks the remaining debris flow (Takahashi 2014). This backwater effect heavily affects the barrier performance, particularly the reduction of debris flow velocity. Therefore, understanding the contribution of slit size and geometry to the velocity reduction of debris flows is equally important. However, the lack of well-controlled and reliable physical modeling results for slit-type barriers that explain the mechanisms for reducing the debris flow velocity and trapping soil debris hampers the understanding, modeling, and prediction of barrier performance regarding debris flows and the design of optimal barrier systems.

This study explored the influence of arrangements (angle and shape) of slit-type barriers on the characteristics of debris flow behavior using small-scale physical model experiments. A set of barrier arrangements was tested by aligning rectangular walls in parallel or in a V-shape at predetermined angles. The barrier was installed in a flow channel, in which debris flows were consistently reproduced using a sand-water mixture and a sand-boulder-water mixture. The velocity reduction and trap ratio were monitored over the course of the experiments, and the obtained results were analyzed to examine the performance of the barrier arrangements. The effect of the presence of large boulders was additionally explored with the debris flows produced using the sand-boulder-water mixture. The performance of slit-type barriers was discussed with respect to two major factors—velocity reduction and trap ratio.

### Experimental program

#### Experimental setup

A rectangular-shaped acrylic flow channel was designed for this study, as shown in Fig. 1. The flow channel was 0.4 m wide, 0.3 m high, and 1.4 m long; and the slope of the channel can be readily controlled from 0° to 50°. The width of the flow channel was

determined by scaling down the width of a natural channel in Korea (i.e., approximately 10–15 m) by 1/30. As the slope of the channel for landslide model tests is recommended to be steeper than  $10^\circ$  (Gregoretti 2000), the slope of our channel was chosen to be  $15^\circ$  over the course of the experiments.

The Froude (Fr) number, the ratio of inertial forces to the gravitational forces, is widely chosen as an indicator of the similarity validation for physical modeling of open channel flows, including debris flows, since the necessary parameters are relatively straightforward to obtain. The gravitational force is the most dominant force, and the Fr number reflects the interactions between debris flows and structures (Armanini et al. 2011; Choi et al. 2015; Hübl et al. 2009). Based on field data, the majority of previous physical model studies have used the Fr number of 0.5–7.6 and occasionally up to 11 in water-dominant flow conditions for the simulation of channelized debris flows (Choi et al. 2015; Cui et al. 2015; Hübl et al. 2009; Scheidl et al. 2013). In particular, the Fr number larger than 10 has been also frequently adopted to model water-dominant debris flows (e.g., Fr = 11 in Choi et al. 2015). Herein, we chose the Fr number of 11 to reproduce debris flows caused by heavy rainfall in Korea, which are reported to have high velocity. As a result, the velocity of the debris flows just before the colliding barriers in our study was approximately 3 m/s, and the thickness was less than 1 cm.

Time-lapsed images of debris flows were acquired by using two digital cameras (UI-3360CP-C-HQ; IDS Corp.) installed along the channel, one at the upstream and the other at the downstream of the slit-type barriers, as shown in Fig. 1a. The images were captured at the rate of 215 frames per second and with a resolution of  $1024 \times 768$  pixels. The collision and overflow patterns of the debris flows against the barriers were imaged by the a digital camera positioned on the side of the flow channel (Fig. 1a). The acquired images were used to analyze the velocity and the patterns of debris flows before and after passing the slit-type barriers.

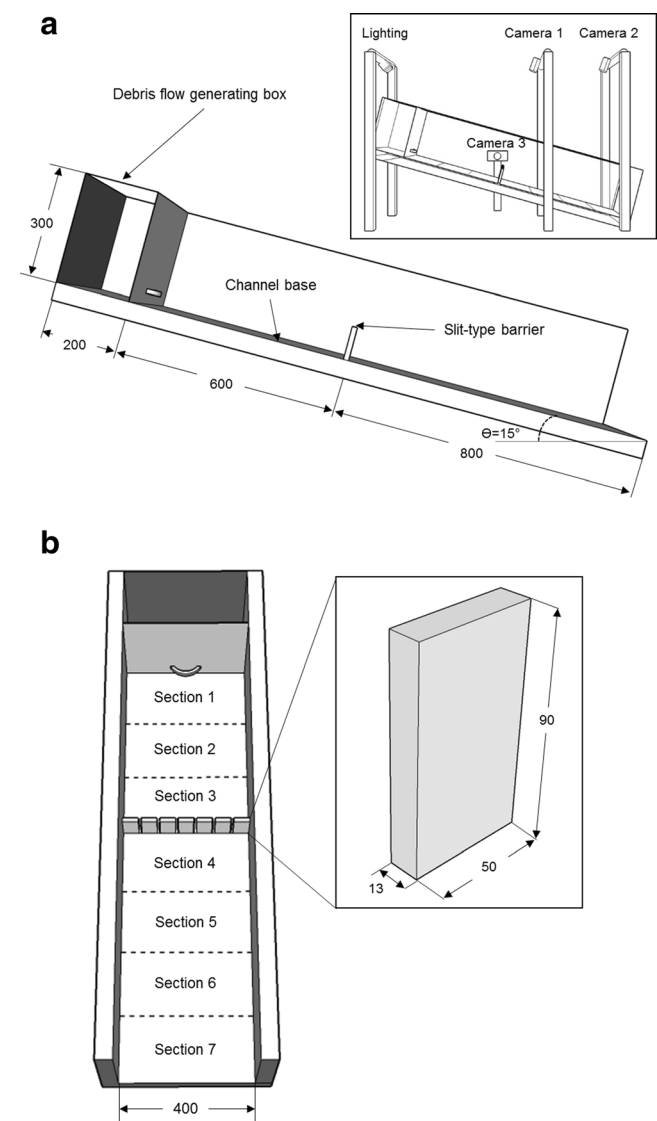
#### Arrangements of slit-type barriers

A set of slit-type barrier arrangements was tested for their performance against debris flows, and all barrier arrangements were composed of a group of seven rectangular walls. Each rectangular wall was made of an acrylic plate that was 50 mm wide, 90 mm high, and 13 mm thick (Fig. 1b). The system of these acrylic walls, of which the angle and spacing can vary, represents a single slit-type barrier. The width of the barrier was determined to be the same as the channel width ( $B$ ). Seven walls were placed in *parallel* with each other, referred to as P-type arrangements. In this P-type arrangement, the angle of the walls to the horizontal direction varied to be  $0^\circ$ ,  $30^\circ$ ,  $45^\circ$ , and  $60^\circ$ , i.e., P00, P30, P45, and P60, respectively. For example, in P00, the seven walls were evenly separated and aligned horizontally (or perpendicular to the flow direction as shown in Table 1). This case is the most widely used arrangement for slit-type barriers. On the other hand, the walls arranged in a *V-shape* were also tested, referred to as V-type arrangements, of which the angles were controlled to be  $30^\circ$ ,  $45^\circ$ , and  $60^\circ$  to the horizontal direction, i.e., V30, V45, and V60, respectively. These V-type arrangements were included in the experiments because they were presumed to be more effective for the trapping of the debris than the P-type arrangements. In addition, the reference test was conducted without a barrier. Table 1 summarizes eight arrangements for the slit-type barrier with different angles and spacing, giving many options to be investigated in this study. When designing the slit-type barrier, the opening ratio was defined in two ways: (a) the projected opening ratio (i.e.,  $\sum b/B$  in Table 1), defined as (the total channel width – the total

projected width of walls)/(the total channel width); and (b) the effective opening ratio (i.e.,  $\sum w/B$  in Table 1), defined as (the flow outlet width)/(the total channel width). The P- and V-type arrangements are presumed to represent the possible extremes, corresponding to the upper and lower limits, respectively.

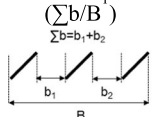
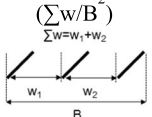






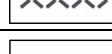
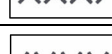
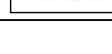
#### Materials and procedures

Two sets of experiments were performed with respect to the debris constituents. One set is the case where the debris was composed of sand and water, referred to as *debris flow* herein; and the other is the case where the debris was composed of a mixture of sand, water, and boulders, referred to as *debris flow with boulders*. In the debris flow tests, a soil-water mixture was prepared by mixing 3.5 kg water and 1 kg dry sand for generating a debris flow. Jumunjin sand, a fairly uniform-sized sand with the mean grain size ( $D_{50}$ ) of 0.6 mm, was used as the solid soil debris, as shown in Fig. 2a, b. The prepared soil-water mixture was placed in the box at the uppermost part of the channel (Fig. 1a). By opening the gate of the box, the soil-water mixture flowed along the



**Fig. 1** Experimental setup: **a** side view and **b** top view. The dimension is in millimeters

**Table 1** Barrier arrangements

Ref.	Number of walls	Effective opening size (w, mm)	Projected opening ratio	Effective opening ratio	Angle of wall (degree)	Arrangement
			$(\frac{\sum b}{B})^1$ 	$(\frac{\sum w}{B})^2$ 		
Ref.	0	400	1	1	-	
P00	7	8.33	0.125	0.125	0	
P30	7	32.37	0.128	0.485	30	
P45	7	40.86	0.220	0.613	45	
P60	7	45.61	0.365	0.684	60	
V30	7	8.57	0.128	0.128	30	
V40	7	12.23	0.183	0.183	40	
V45	7	14.69	0.220	0.220	45	
V60	7	24.37	0.365	0.365	60	

$\sum b$  sum of the projected opening width of channel,  $B$  total width of channel,  $\sum w$  sum of the effective opening width of channel

channel. The two digital cameras above the channel and the digital camera at the side of the channel recorded the movement of the debris flow. When the flow stopped, the solid particles (sand) deposited on the channel were collected from each section and dried to measure their dry masses. The same procedure was applied to all the arrangements of barriers listed in Table 1. For each arrangement, the identical debris flow event was repeated three times to confirm repeatability and to obtain average results.

Most natural debris contains a variety of large solid particles, such as boulders and woods as well as fines, such as clays and silts (Iverson 1997; Nasmith and Mercer 1979). Boulders that usually have a big momentum show a pronounced effect on the physical and hydraulic characteristics of debris flows. For instance, the size of such large debris is reported to range from cobbles of 20 cm to boulders larger than 50 cm in Korea (Jeong et al. 2015) and boulders of 25–201 cm in the USA (Scott et al. 1995).

Accordingly, a set of experiments was conducted to explore how and to what extent the presence of boulders affects the barrier performance. For preparation of the solid debris, two kinds of boulder-like particles were used. One is a rod-shaped gravel with a width of approximately 18 mm and length of 50 mm (i.e., an angular boulder, hereafter referred to as AB and shown in Fig. 2c). The other particles are spherical glass beads with a diameter of 16 mm (i.e., a round boulder referred to as RB and shown in Fig. 2d). Thereby, the diameters of the maximum inscribed circles ( $d_{max}$ ) were approximately 18 mm for the angular boulders and 16 mm for the round boulders, respectively. The size of the boulder used in the model tests was chosen to represent the boulders in natural debris of 50 cm, applying the scaling ratio of 1/30. Six debris samples were prepared, in which the boulders were mixed with sand at mass ratios of 5, 9, and 13%, and referred to as RB05, RB09, RB13, AB05, AB09, and AB13, respectively. In the debris flow tests with boulders, the wall arrangements of P00, V30, and V40 were tested, and the other experimental conditions and

procedures, such as the channel slope, were kept the same as in the debris flow tests. For each arrangement and each debris sample, the identical debris flow event was repeated three times to confirm repeatability and to obtain consistent results. All of the cases are summarized in Table 2.

**Image analyses and data reduction**

The particle tracking velocimetry (PTV) code (Thielicke and Stamhuis 2010) was used to analyze the acquired time-lapsed images and to estimate the velocity of the debris flows. The velocity was calculated based on the displacements of moving targets per frame. Blue glass beads with 5 mm diameter were used as the targets, and these glass beads were mixed with the sand-water mixture prior to the generation of the debris flow events. Because the glass beads had a similar specific gravity as the Joomunjin sand (i.e.,  $G_s$  = approximately 2.5), it is reasonable to presume that most of the beads moved together with the sand particles, which was later confirmed by inspecting the recorded images. The following procedure was conducted to extract the representative velocity of a debris flow passing each section: (1) the blue color was first extracted from the raw images; (2) such images were converted to gray scale, such that the positions of the glass beads were distinctly marked in white color; (3) the velocity of each white dot was estimated using the PTV code; and (4) lastly, the representative velocity of the debris flow was obtained by averaging the velocity values of the dots.

**Results and analyses**

Two factors, velocity reduction and trap ratio, were chosen for evaluating the performance of the arrangements of the slit-type barriers. The reasons for choosing these factors are as follows. First, as most of debris flows that occurred in Korea are caused by extreme rainfall, the

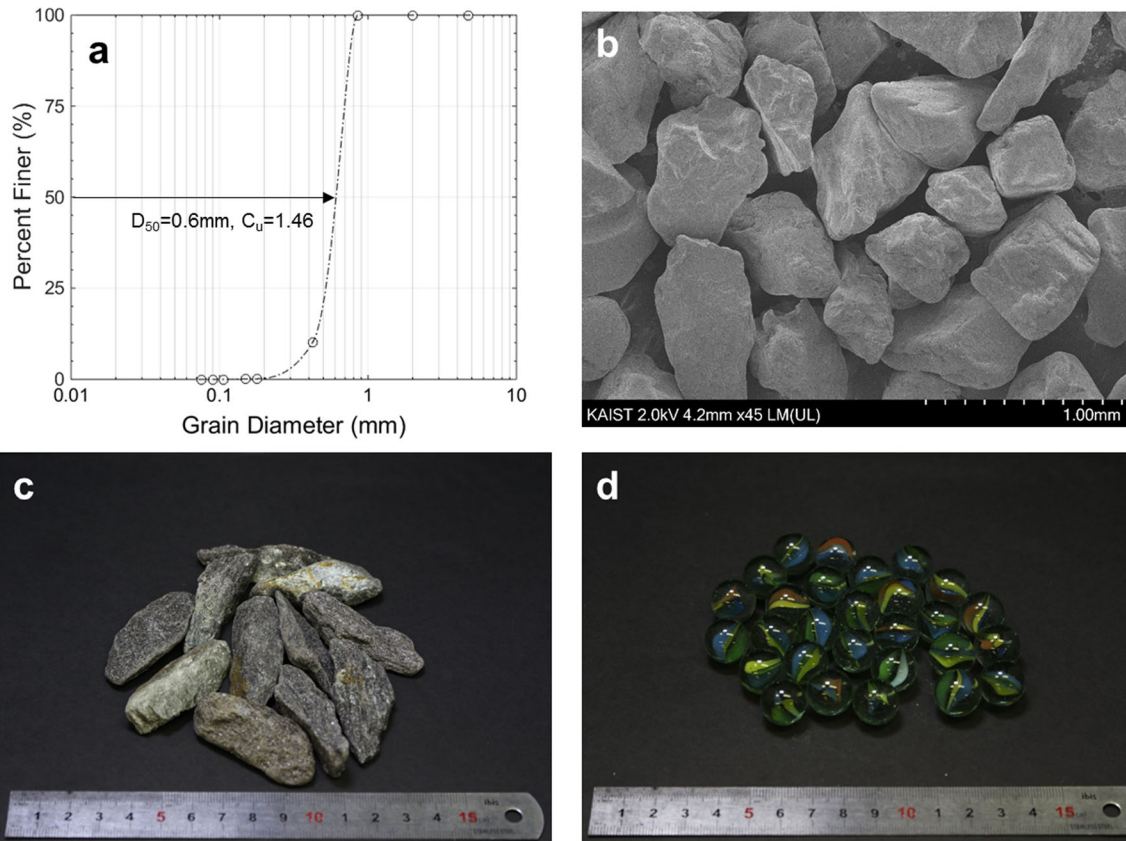


**Fig. 2** Properties of solid debris: **a** the grain size distribution of Jumunjin sand, **b** a SEM image of Jumunjin sand, **c** a digital picture of angular boulders, and **d** a digital picture of round boulders

velocity of these water-dominant debris flows is fairly fast. For instance, the maximum debris flow velocity in Woomyeon Mountain is approximately 28 m/s (Jeong et al. 2015). As a result, the velocity reduction of such debris flows, which is one of the important roles of debris flow barriers, was monitored. Second, as a debris flow flows downstream, the channel bottom is unavoidably scoured by solid debris, in particular by massive debris, such as cobbles and boulders. If these sorts of massive debris can be removed by the barriers, the impact of the debris flow, in terms of kinetic energy or momentum of mass, is presumed to significantly diminish. Therefore, the trapping of solid debris by the debris flow barriers was examined.

### Results of debris flow tests

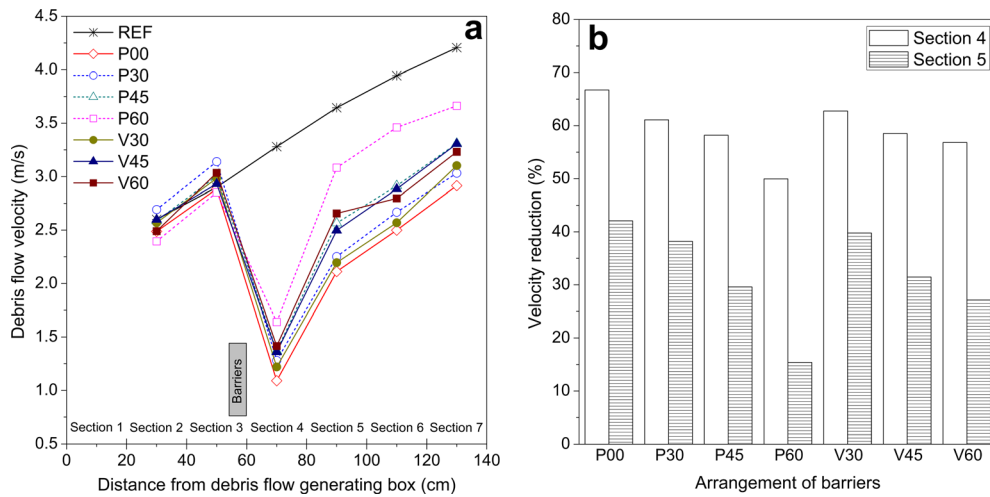
#### Velocity reduction

Figure 3a shows the changes in velocity of the debris flows along the channel. All debris flows started from the same initial spot, the location of the door of the debris flow generating box (see Fig. 1a). Therefore, the travel distances of a debris flow were 10, 30, 50, 70, 90, 110, and 130 cm, at the mid-point of sections 1, 2, 3, 4, 5, 6, and 7, respectively. In the reference case with no barriers, the average velocity was measured as 2.6 m/s at section 2, where the travel distance was 30 cm (or 30 cm away from the initiation spot). The

**Table 2** Composition of tested debris flow

Case	Composition	Water (L)	Sand (kg)	Boulder (kg)	Tested arrangement
Sand	Sand 100%	3.5	1	–	REF, P00 P30, V30 P45, V45 P60, V60
AB05	Sand 95% + boulder 5%	3.5	1	0.053	P00, V30, V40
AB09	Sand 91% + boulder 9%	3.5	1	0.099	
AB13	Sand 87% + boulder 13%	3.5	1	0.149	
RB05	Sand 95% + boulder 5%	3.5	1	0.053	
RB09	Sand 91% + boulder 9%	3.5	1	0.099	
RB13	Sand 87% + boulder 13%	3.5	1	0.149	





**Fig. 3** Results of debris flow velocity for barrier arrangements: **a** variations of debris flow velocity along the channel and **b** velocity reduction in sections 4 and 5

average velocity increased to approximately 4.5 m/s at section 7, which was 150 cm away from the initiation spot. In all cases with the slit-type barriers, it was observed that the presence of a barrier significantly reduced the velocity of the debris flows (Fig. 3a). To compare the performance of different barrier arrangements

further, the velocity reductions at sections 4 and 5, where their travel distances were 70 and 90 cm and the locations were 10 and 30 cm further away from the barrier, were calculated in comparison to the reference case. Accordingly, the velocity reduction was defined as  $(V_{\text{barrier}} - V_{\text{REF}})/V_{\text{REF}}$ . In particular, caution was taken

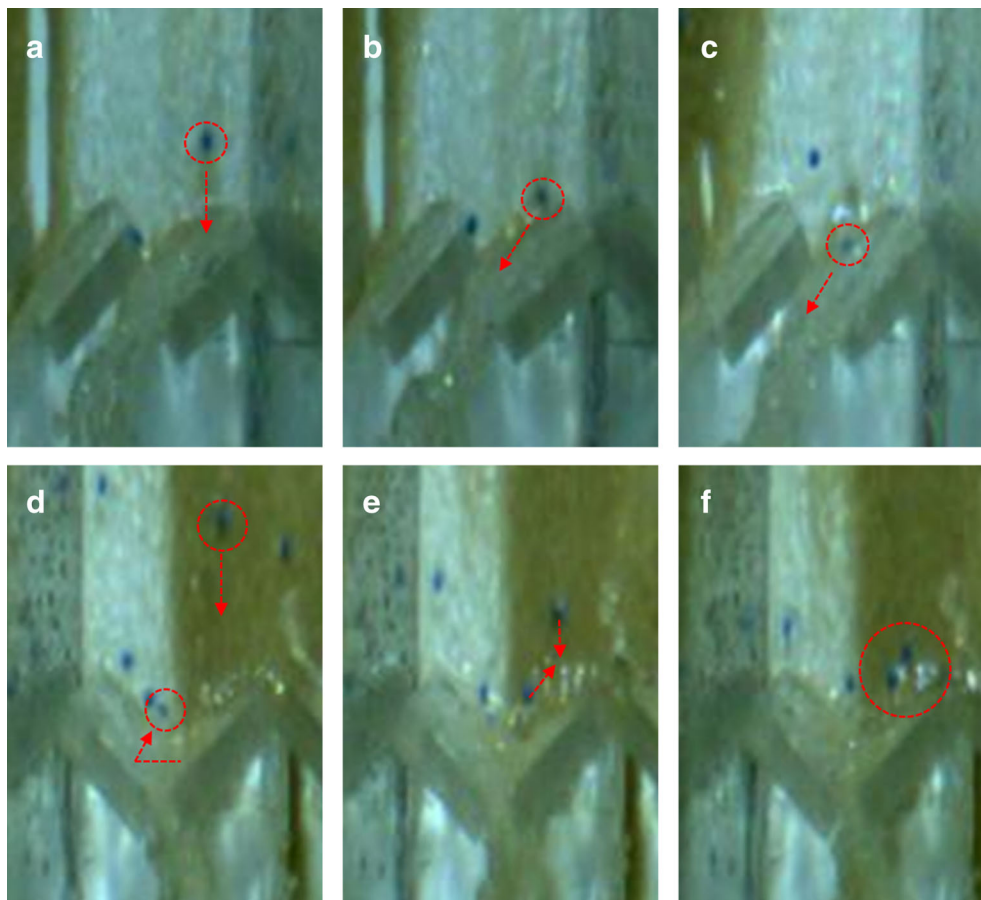


**Fig. 4** Collision behaviors of debris with the P30 and V30 barriers. **a–c** The time-elapsing images of the top views of P30. The debris and blue beads move following a curved path through slits. **d–f** The time-elapsing images of the top views of V30. The debris and beads bounce back from a wall and collide with the following debris. The time interval between images is 9.3 ms

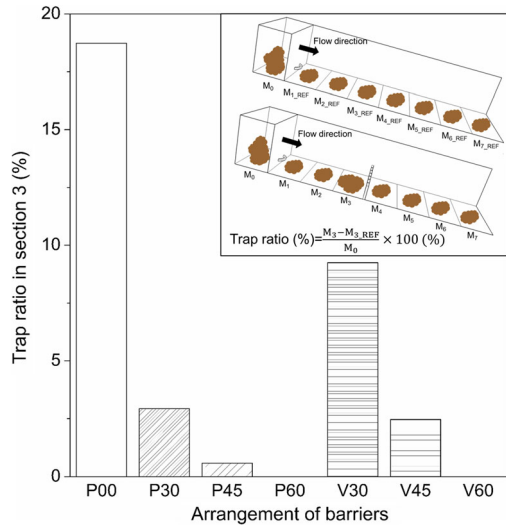


Fig. 5 Results of trap ratio in section 3

to estimate the velocity for section 4 because of the turbulent flows caused by the slit-type barriers and the overflows.

Figure 3b shows the velocity reductions with respect to the barrier arrangements. Arrangement type P00 showed the greatest reduction in velocity by 67% (or 1.09 m/s) at section 4 and 42% (or 2.1 m/s) at section 5 among the seven arrangements, and P00 had the smallest projected opening width. The smallest velocity reduction was observed in P60 that had the largest projected opening width. For both sections 4 and 5, it was clearly found that the extent of velocity reduction diminished as the angle of the barrier

increased; e.g., velocity reductions in section 5 were 42% in P00, 38% in P30, 30% in P45, and 15% in P60, respectively. A similar trend, an increase in velocity reduction with a decrease in the angle of the barrier, was observed for the V-type arrangements, i.e., 40% in V30, 31% in V45, and 27% in V60 for the velocity reduction in section 5 (Fig. 3b). The trends in velocity reduction in section 4 are also consistent with those in Section 5. This is because the projected opening ratio decreased as the barrier angle decreased. Therefore, this result indicates that the velocity reduction is inversely proportional to the projected opening ratio.

In particular, the V-type arrangements rendered a greater velocity reduction than the P-type arrangements for a given angle. Figure 4 demonstrates the collision behaviors of debris with the P- and V-type barriers (also see Online Resources 1 and 2). In any debris flow event, it was observed that the debris was widely distributed, resembling a shooting star with a head, main body, and tail. After the impact of the head of the debris on the walls, the collided debris bounced back upstream or converged at the tips of the V-type walls. This led to a secondary collision with the following debris tail coming from behind. This secondary collision was more pronounced in the V-type arrangements than in the P-type arrangements due to a bottleneck effect where the debris flow converged (see Fig. 4). This led to a greater velocity reduction. These results confirm that such secondary collisions by the bottleneck effect have a significant impact on the velocity reduction.

Trap effect

The trap ratio was estimated as the ratio of the dry soil mass trapped at section 3 ( $M_3$ ) to the initial dry soil mass that flowed

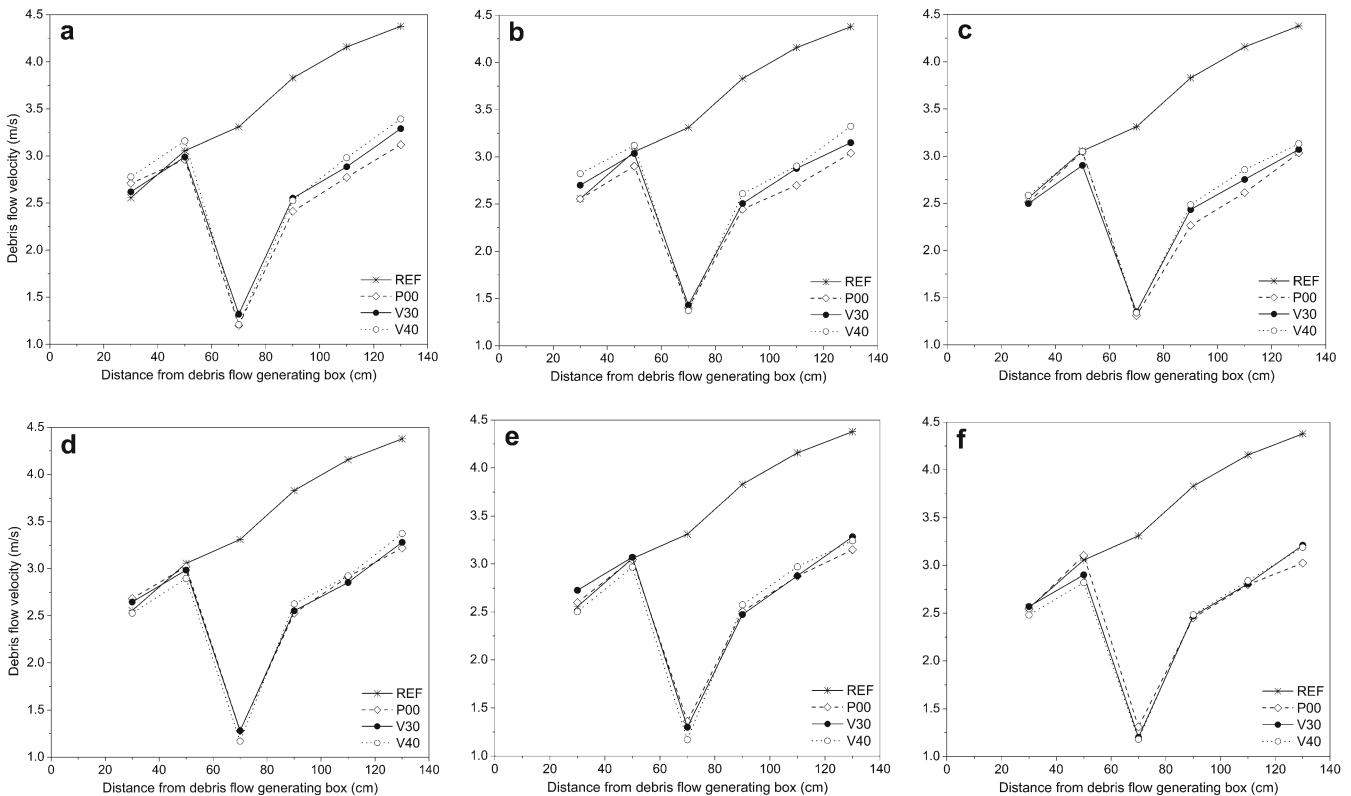
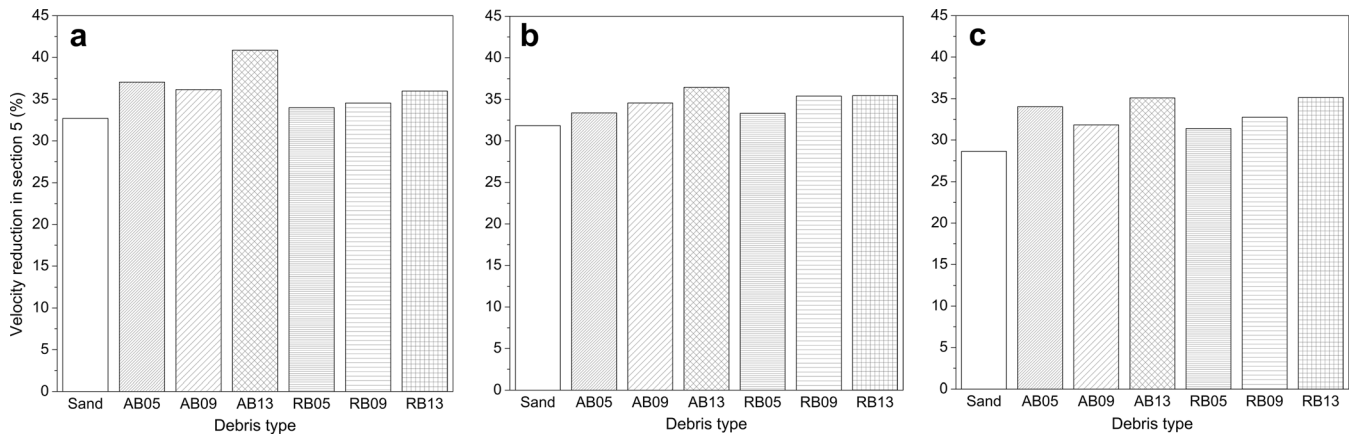


Fig. 6 Variations in velocity of the debris flow test with boulders: a AB05, b AB09, c AB13, d RB05, e RB09, and f RB13



**Fig. 7** Velocity reduction of debris flows: **a** P00 barrier, **b** V30 barrier, and **c** V40 barrier

as a source debris flow ( $M_o$ ), as depicted in Fig. 5. In our study, there was a consistent amount of soil mass deposited along the channel in the reference case, where no barrier was deployed. In order to examine the sole effect of barriers on the trapping of debris, the dry soil mass deposited at section 3 in the reference case without barriers ( $M_{3\_REF}$ ) was subtracted from the dry soil mass trapped by barriers at section 3 ( $M_3$ ) to calculate the trap ratio, i.e., trap ratio =  $(M_3 - M_{3\_REF})/M_o$ .

Figure 5 shows the calculated trap ratios for the tested barrier arrangements. Similar to the results for the velocity reduction, Poo case showed the best trap ratio of 19% among the tested barriers, and the trap ratio decreased with an increase in wall angle for the P-type arrangements (e.g., 3% for P30, 0.58% for P45, and 0% for P60). For V-type arrangements, the same trend of increasing trap ratio with decreasing wall angle was observed (e.g., 9% for V30, 2.5% for V45, and 0% for V60). The V-type arrangements exhibited larger trap ratios than the P-type arrangements for the same angle and projected opening ratio. It implies that the effectiveness of the secondary collision between the head and tail of the debris or collided debris at the tips of the V-type arrangements heavily affected the trap ratio. In particular, when the wall angle was 60° in the P- and V-type arrangements, no trap was observed (i.e., trap ratio = 0%) because the secondary collisions among the debris were not significant enough to diminish the energy of the debris

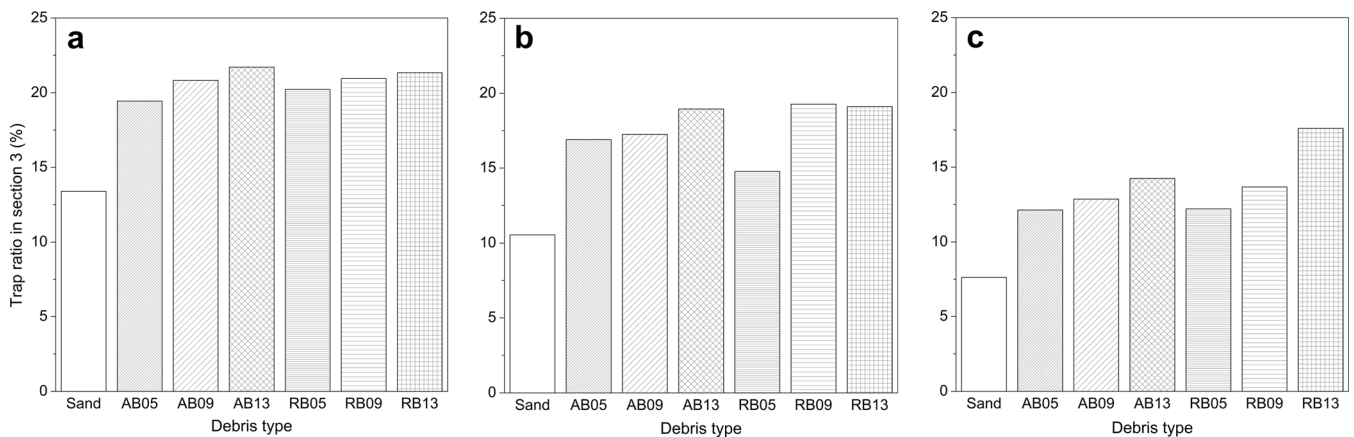
flow to cause the deposition of debris. Apparently, the tested barrier arrangements produced similar results for the trap ratio and velocity reduction, which indicates that these two parameters mutually share the same physical causality.

#### Results of debris flow tests with boulders

This section provides the test results for the flows of the mixture of sand, water, and boulders (hereafter, debris flows with boulders). For the performance evaluation of the debris flows with boulders, three barrier arrangements of Poo, V30, and V40 were tested, in which the opening size was just small enough to occlude the whole boulders. These types of barriers were selected because Poo was more efficient than any other barriers, and the V-type arrangements showed better performance than P-type arrangements.

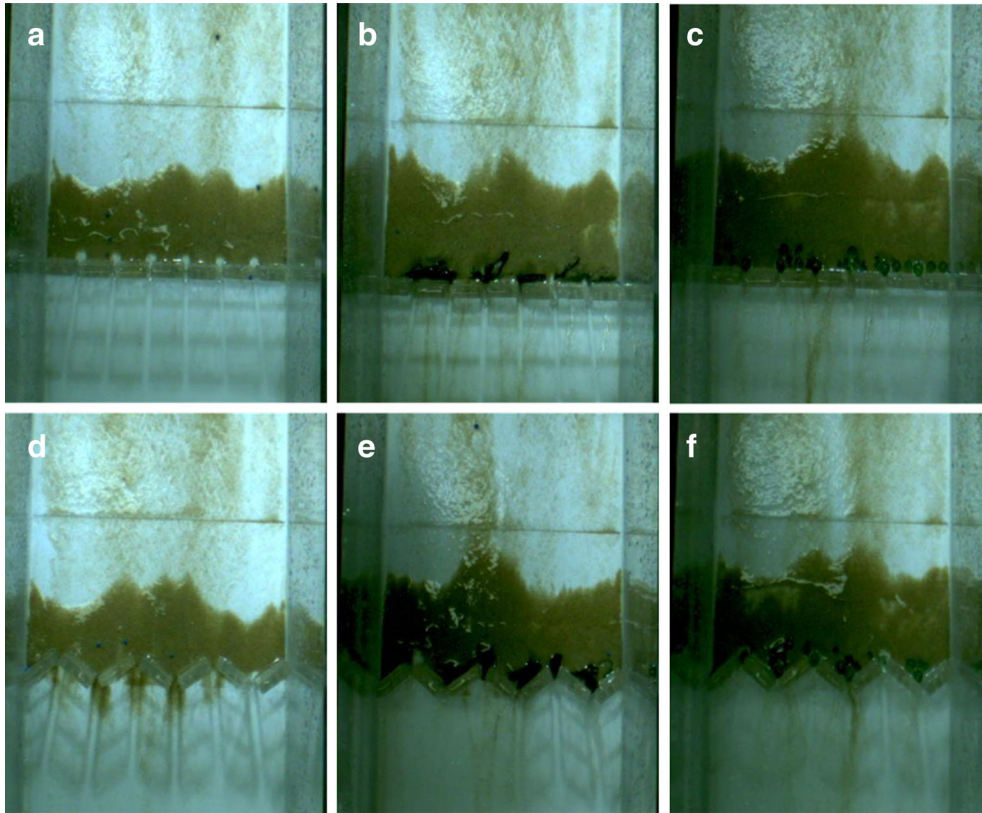
#### Velocity reduction

Figure 6 shows the velocity of the debris flows containing different fractions of boulders (see Table 2). In all debris flow tests with boulders, the presence of barriers significantly reduced the velocity. It was worth noting that the extent of the velocity reduction was consistent regardless of the arrangement of the barrier, in particular for RB13, RB09, and RB05. This is probably because the boulders were all trapped by the Poo, V30, and V40 barriers, which blocked the tail of the debris from subsequently flowing.



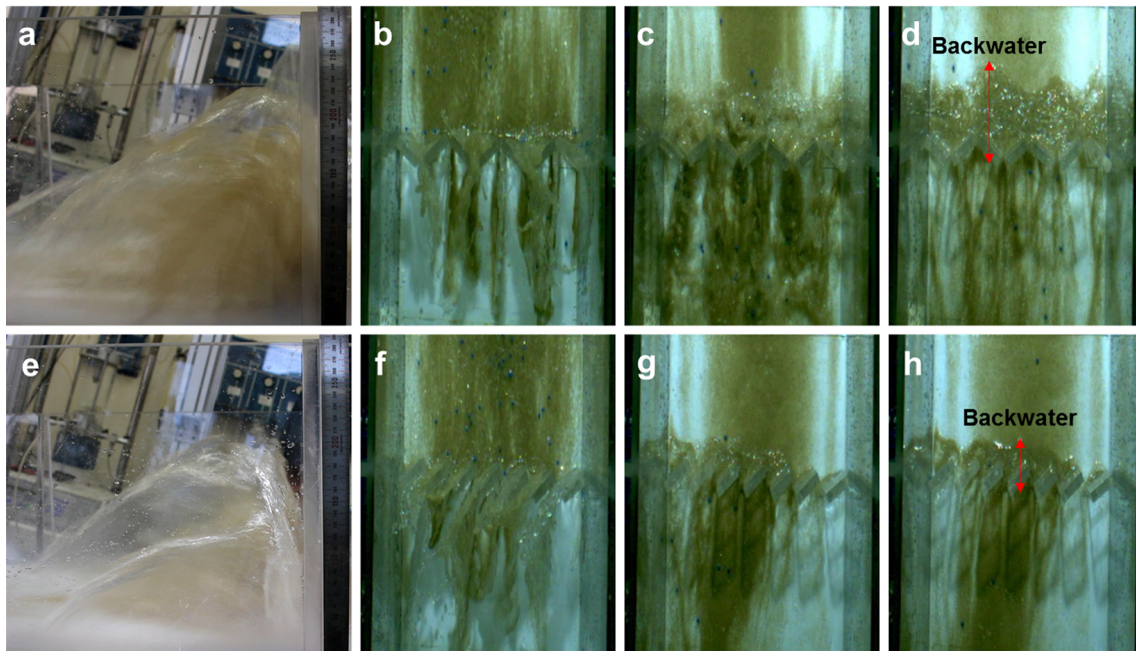
**Fig. 8** Trap ratio of debris flows: **a** P00 barrier, **b** V30 barrier, and **c** V40 barrier





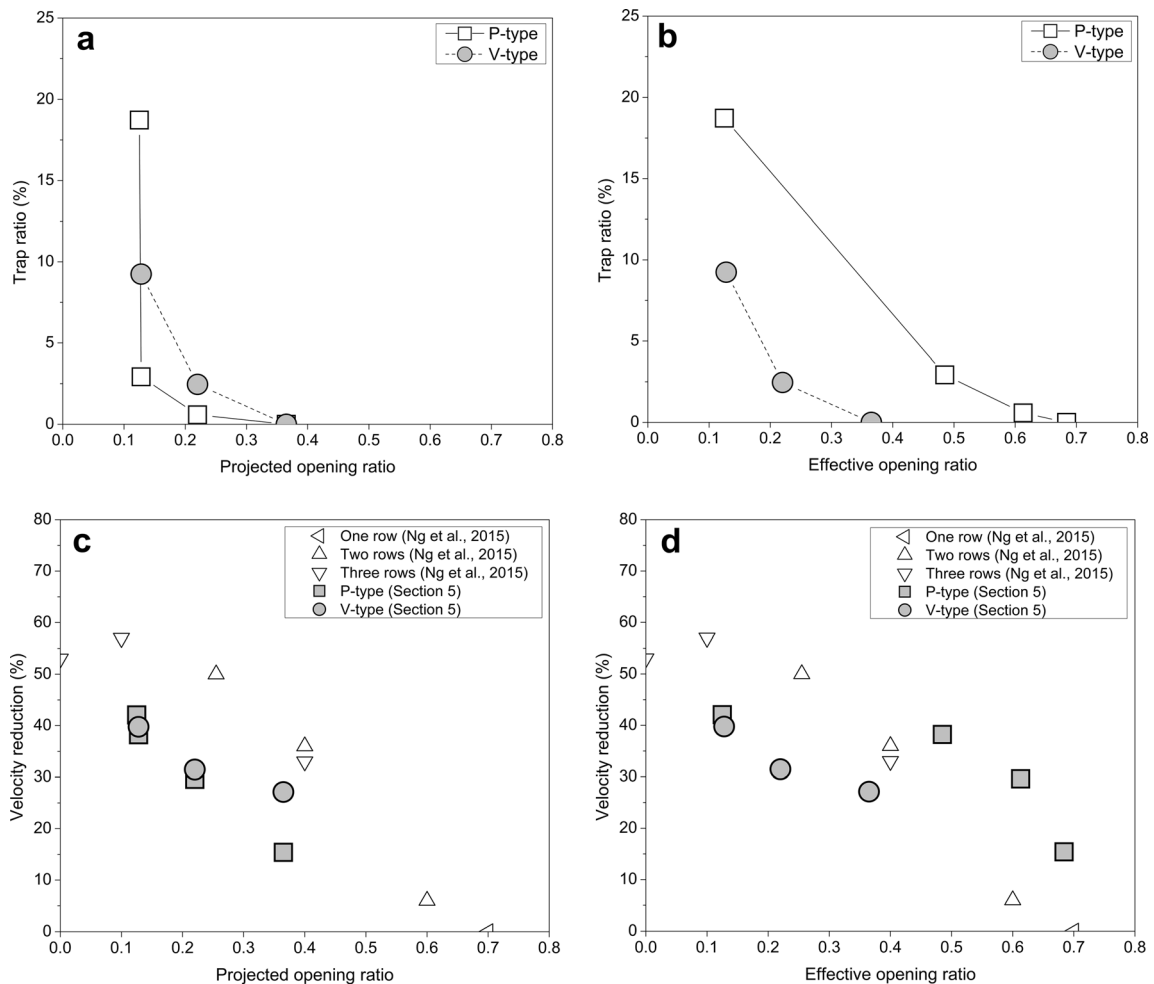
**Fig. 9** Digital images of trapped debris in front of barriers: a P00 with only sand, b P00 with AB13, c P00 with RB13, d V30 with only sand, e V30 with AB13, and f V30 with RB13

Figure 7 shows the velocity reductions for different fractions of boulders in the debris for a given barrier arrangement. While the velocity reductions in section 4 appeared somewhat inconsistent because of turbulent behavior and overflows, priority was given to



**Fig. 10** Digital images of bottleneck and backwater effects observed with sand debris flows: a the section view of V30, b–d the time-elapsing images of the top views of V30, e the section view of P30, and f–h the time-elapsing images of the top views of P30. In d and h, the red arrows indicate the backwater effects generated during the debris flow events





**Fig. 11** Variations in trap ratio and velocity reduction of sand debris with respect to opening ratios: **a** the trap ratio versus the projected opening ratio, **b** the trap ratio versus the effective opening ratio, **c** the velocity reduction versus the projected opening ratio, and **d** the velocity reduction versus the effective opening ratio

the velocity reduction results in section 5. In all cases, the presence of boulders reduced the velocity more than in the cases with only sands. For the debris containing 13% angular boulders (AB13), the additional velocity reduction was 8, 4, and 6% for Poo, V30, and V40 in comparison to the cases with only sand (Fig. 7). As the debris contained more boulders, the extent of the velocity reduction also became greater. The velocity reduction for the Poo barrier increased as the angular boulder fraction increased (e.g., 37% for PooAB05, 36% for PooAB09, and 41% for PooAB13). A similar trend was observed for the round boulders (e.g., 34% for PooRB05, 35% for PooRB09, and 36% for PooRB13). For the V30 and V40 arrangements, the same observations were consistently confirmed. When comparing the effect of the angularity of boulders, the angular boulders caused slightly more reduction in velocity than the round boulders did though the differences were not pronounced. With a smaller amount of boulders, there was a larger effect of the angularity of the boulders. This is because the slender shape of the angular boulders led to a more efficient blockage of the slit openings between the walls.

#### Trap effect

Figure 8 shows the trap ratio caused by blocked boulders considering the deposited sand of the reference case. Figure 9 shows the

pictures of the deposited sand and boulders for the Poo and V30. In all cases, the presence of boulders increased the trap ratio to values greater than in the cases with only sands. The presence of boulders increased the trap ratio more than 6% in the Poo barrier (Fig. 8a). Similar to the velocity reduction, an increase in the boulder fraction led to an increase in trap ratio in all barrier types (e.g., 19% for PooAB05, 21% for PooAB09, 22% for PooAB13, 20% for PooRB05, 21% for PooRB09, and 21% for PooRB13). The barrier arrangements had an influence on the trapping of the debris; Poo had the greatest trap ratios, followed by V30. V40 showed the lowest trap ratios. The noticeable effect of the angularity of the boulders on the trap ratio was not observed in this study.

#### Discussion

##### Backwater effect on debris trapping and velocity reduction

It was found that the debris trapping was significantly affected by the *backwater effect*. When analyzing the recorded images of debris flows, it was observed that the body and tail of the debris flow were mostly trapped, while the front of the debris flow passed without any trapped solids because of the prevailing amount of water over the solid debris. Part of the debris flow bounced back from the walls and collided with the following body and tail, as

captured in Fig. 10. This is referred to as the *backwater effect*, which can be considered as the secondary collision among the debris. This led to the reduction of kinetic energy and velocity and, eventually, caused deposition and trapping of the debris by a barrier. This backwater effect became more pronounced as the outlet width became narrower (i.e., the bottleneck effect); therefore, more significant backwater effect and thus more debris trap occurred in the V-type barriers than in the P-type barriers owing to the smaller width of the flow outlet or the smaller effective opening ratio, as demonstrated in Fig. 10 (see Online Resources 1 and 2). It was found that the effective opening ratio was better correlated to the magnitude of the backwater effect and thus to the trap ratio rather than the projected opening ratio, as shown in Fig. 11a, b.

Overall, for the projected opening ratio ( $\Sigma b/B$ ) of 0.125–0.365 and the effective opening ratio ( $\Sigma w/B$ ) of 0.125–0.684 tested in this study, a velocity reduction of approximately 15–42% was observed in section 5, as shown in Fig. 11c, d. Our experimental results were fairly consistent with the results of Ng et al. (2015) though their velocity reduction was greater than ours, which is possibly attributed to their particular arrangements with multiple rows. While the velocity reduction generally decreases with increases in the opening ratio, the correlations with the projected opening ratio and the effective opening ratio are somewhat complex (Fig. 11c, d). The velocity reduction appears to be linearly correlated with the projected opening ratio for the P-type arrangements though the V-type arrangement was not well correlated with the projected opening ratio. Instead, the overall velocity reduction result exhibits a fairly consistent decreasing trend with an increase in the effective opening ratio, though it is a wide band (Fig. 11d). Because the greater velocity reduction in V60 against P60 is in part attributed to the more pronounced secondary collision and backwater effect, it is presumed that the effective opening ratio would be better correlated to the velocity reduction, as it is to the trap ratio.

In addition, no debris was trapped when the angle of walls was 60° in either the P- and V-type barriers. This implies that the angle of the barrier walls needs to be smaller than 60° to benefit from debris trapping mechanisms. Further, the projected opening ratio ( $\Sigma b/B$ ) of 0.125–0.128 was found to be optimal in this study. In previous literature (Ikeya and Uehara 1980; Wenbing and Guoqiang 2006), the projected opening ratio ( $\Sigma b/B$ ) of 0.2–0.6 was suggested as an optimal range for slit-type barriers resulting in the greatest reduction of debris flow intensity (e.g., discharge, velocity, and density). The particle size of the debris used in our study (e.g., approximately 0.52 mm) was smaller than in those previous studies (100–400 mm in Ikeya and Uehara 1980; 200 mm in Wenbing and Guoqiang 2006). As a result, it appears that for a given projected opening size, the trap ratio and velocity reduction can differ depending on the physical characteristics of the debris and its flow. This is further corroborated by the results of the debris flows with boulders, as described in the following section.

The experiment condition was scaled down to 1:30 with the Froude number of 11, as described in the “Experimental setup” section. In all experiments, the debris flows consistently approached the wall with the velocity of approximately 3 m/s and the thickness less than 1 cm, which are equivalent to 18 m/s and 27 cm, respectively, if upscaled with the Froude number of 11. While the channel width, barrier size, and slit opening size can be upscaled by a factor of 30, the barrier arrangements tested here, including the opening ratio, wall angle, and wall arrangement, can

be kept constant. If upscaled, therefore, for the tested barrier arrangements, the observed tendencies in velocity reduction and trap ratio are expected to be valid in a qualitative way.

### Effect of the presence of boulders

Figure 12 highlights the presence of boulders in the debris, where the velocity reduction and the trap ratio clearly increased with an increase in the boulder fraction. As the barriers retained the boulders, such boulders occluded the slits and the following parts of the debris were blocked. The presence of the boulders rendered a greater contribution when the angle of the wall and the opening ratio were greater. For instance, the V40 barrier, having the widest opening size among P00, V30, and V40 barriers, showed the greatest increase in the trap ratio with an increase in the boulder fraction (Fig. 12b). In the present study, the ratio of each slit size  $w$  to the diameter of the maximum inscribed circles within debris particles  $d_{\max}$  (or  $w/d_{\max}$  ratio) ranged from 0.52 to 0.76 for the round boulders (RB) and 0.46 to 0.68 for the angular boulders (AB); in all cases, for both RB and AB, all the boulders were thus trapped by the barriers owing to the small slit sizes. For the tested  $b/d_{\max}$  ratios, the trap ratio was found to be in the range of 12–22%, in which the mass of the boulders was excluded in the trap ratio calculation. Watanabe et al. (1980) showed a reduction of the debris flow volume by more than 50% during peak time for a  $b/d_{\max}$  ratio less than 2. Considering the mass of trapped boulders,

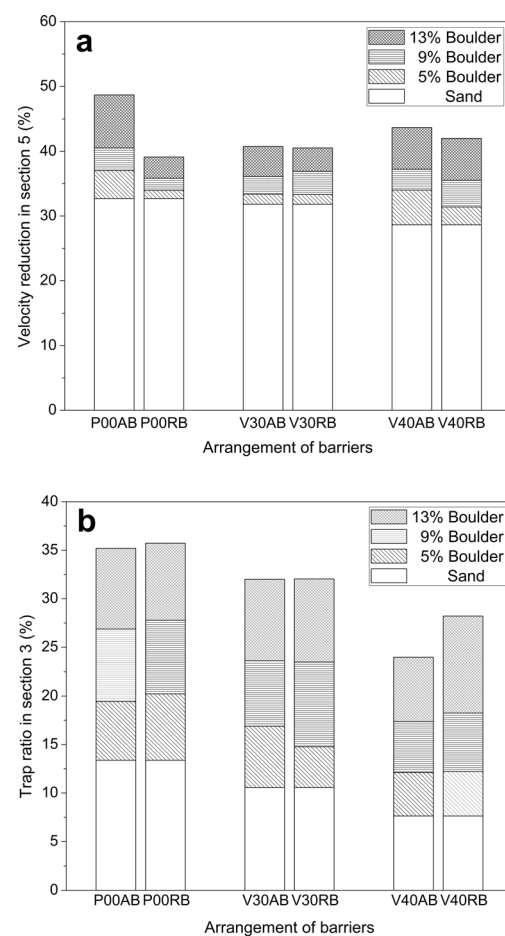
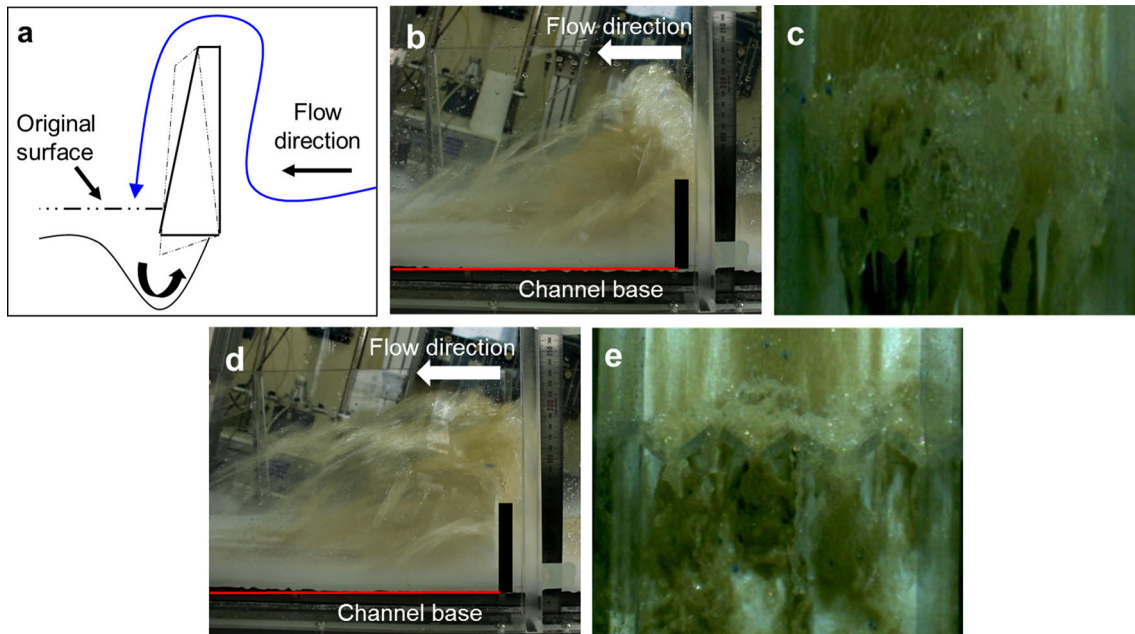


Fig. 12 Effect of boulder fraction in debris flows: a velocity reductions and b trap ratios



**Fig. 13** Overflow patterns in P00 and V30 barriers: a overview of an overflow pattern, b the section view of P00, c the top view of P00, d the section view of V30, and e the top view of V30

our results are consistent with those in previous studies while we observed that all boulders were trapped at the slits because the  $b/d_{\max}$  ratio was less than 2.

#### Observations of overflow magnitude

The overflow phenomenon is expected to occur unavoidably when the amount of debris flow exceeds the capacity of the barriers, as shown in Fig. 13a. When part of the debris flow overflows to the downstream over the barrier, the overflowed debris unavoidably causes the scouring of the ground surface and degrades the structural stability of the barrier, possibly causing overturning of the barriers (see Fig. 13a) (Kim et al. 2013; Pan et al. 2012). In this section, the roles of the barrier arrangements in the magnitude of the overflows were additionally examined using our test results.

Comparing V30 against P00, the V30 barrier caused a smaller overflow than the P00 barrier, as shown in Fig. 13. While the height of overflow was similar in both cases (Fig. 13b, d), most of the overflow debris in P00 dropped directly behind the barriers, as shown in Fig. 13b. However, most of the overflow debris in V30 was dispersed over a wide area from the barrier, as shown in Fig. 13d. This indicates that the scouring impact by the overflow debris in V30 would be less than that in P00. The surface of the P00 barrier was entirely covered with the overflow debris (Fig. 13c), whereas only the tips of the V30 barrier were covered with overflow debris (Fig. 13e). This indicates that the amount of overflow debris in V30 was smaller than that in P00. Accordingly, it is expected that the magnitude of overflow will decrease as the angle of the walls increases. This result is also consistent with the previous study using baffles (Ng et al. 2015), where they reported that when the degree of the transverse blockage increased from 20 to 30%, the overflow height increased from  $1.4H$  to  $1.6H$ , where  $H$  is the wall height. Accordingly, the open-type barriers are expected to cause less overflow compared to the closed-type barriers.

The present experimental results would provide baseline data for insights to overflow reduction with respect to the arrangement

of slit-type barriers and for the optimum design of slit-type barriers against debris flow.

#### Conclusion

This study investigated the influence of new arrangements (angle and shape) of slit-type barriers on the characteristics of water-dominant debris flows via small-scale model experiments. The debris, made of the sand-water mixture and sand-boulder-water mixture, were reproduced and flowed against the slit-type barriers, varying the angle and shape of barrier arrangements; and the velocity reduction and trap ratio were monitored to examine the performance of the barrier arrangements. The salient findings are as follows:

- The extent of the velocity reduction grew as the angle of the barrier wall decreased and the opening ratio decreased. The secondary collision, particularly the backwater effect was more pronounced in V-type arrangements than in P-type arrangements due to the narrower outlet, hence the more bottleneck effect.
- Secondary collisions caused by the backwater effect that often occurred in front of the barrier led to the deposition and trapping of the debris. The V-type barriers showed a higher trap ratio than the P-type due to the smaller effective opening ratio and the larger backwater effect. The trap ratio decreased with an increase in the wall angle for the P- and V-type arrangements; it was found that the angle of the barrier walls smaller than  $60^\circ$  was required to benefit from debris trap mechanisms.
- As the debris contained more boulders, the extent of the velocity reduction also became greater. Similar to the velocity reduction, an increase in boulder fraction led to an increase in trap ratio in all barrier types. However, the noticeable effect of the angularity of the boulders on the trap ratio was not observed in this study.



- The magnitude of the overflow decreased as the angle of the walls and the effective opening ratio increased. The scouring impact by overflow debris is expected to decrease with increases in the wall angle and the effective opening ratio.

The present study shows that the risk of damage by debris flows can be effectively reduced by a slit-type barrier via the reduction of flow velocity and the trapping of the debris mass. The experimental results would provide baseline data for insights into the performance of slit-type barriers and for the optimum design of slit-type barriers against debris flow.

#### Acknowledgements

This research was supported by a grant (13SCIPSo4) from Smart Civil Infrastructure Research Program funded by the Ministry of Land, Infrastructure and Transport (MOLIT) of Korea government and Korea Agency for Infrastructure Technology Advancement (KAIA) and by the Basic Science Research Program through the National Research Foundation of Korea (NRF) funded by the Ministry of Science, ICT Future Planning (2014R1A1003419).

#### References

- Armanini A, Larcher M, Odorizzi M (2011) Dynamic impact of a debris flow front against a vertical wall. 5th International conference on debris-flow hazards mitigation: mechanics, prediction and assessment, Padua, Italy, 14–17 June, pp 1041–1049
- Choi CE, Ng CW, Au-Yeung SCH, Goodwin GR (2015) Froude characteristics of both dense granular and water flows in flume modelling. *Landslides* 12:1197–1206. doi:10.1007/s10346-015-0628-8
- Cui P, Zeng C, Lei Y (2015) Experimental analysis on the impact force of viscous debris flow. *Earth Surf Proc Land* 40:1644–1655. doi:10.1002/esp.3744
- Evans SG (1982) Landslides and surficial deposits in urban areas of British Columbia: a review. *Can Geotech J* 19:269–288
- Gregoretti C (2000) The initiation of debris flow at high slopes: experimental results. *J Hydraul Res* 38:83–88. doi:10.1080/00221680009498343
- Hübl J, Suda J, Proske D, Kaitna R, Scheidl C (2009) Debris flow impact estimation. 11th International symposium on water management and hydraulic engineering, Ohrid, Macedonia, 1–5 September, pp 1–5
- Hungr O, Morgan G, Kellerhals R (1984) Quantitative analysis of debris torrent hazards for design of remedial measures. *Can Geotech J* 21:663–677
- Ikeya H, Uehara S (1980) Experimental study about the sediment control of slit Sabo dams. *Jpn Erosion Control Eng Soc* 114:37–44
- Iverson RM (1997) The physics of debris flows. *Rev Geophys* 35:245–296
- Jakob M, Hungr O, Jakob DM (2005) *Debris-flow hazards and related phenomena*. Springer, Berlin
- Jeong S, Kim Y, Lee JK, Kim J (2015) The 27 July 2011 debris flows at Umyeonsan, Seoul, Korea. *Landslides* 12:799–813

- Kim Y, Nakagawa H, Kawaike K, Zhang H (2013) Study on characteristic analysis of closed-type Sabo dam with a flap due to dynamic force of debris flow. *Annals of the Disaster Prevention Research Institute, Kyoto University, Japan*
- Lister D, Morgan G, Vandine D, Kerr J (1984) Debris torrents along Howe Sound, British Columbia. 4th International Symposium on Landslides, Toronto, Canada, pp 649–654
- Nasmith H, Mercer A (1979) Design of dykes to protect against debris flows at Port Alice, British Columbia. *Can Geotech J* 16:748–757
- Ng CW, Choi C, Song D, Kwan J, Koo R, Shiu H, Ho KK (2015) Physical modeling of baffles influence on landslide debris mobility. *Landslides* 12:1–18. doi:10.1007/s10346-014-0476-y
- Pan HL, Huang JC, Wei LQ, Ou GQ (2012) A study on scouring laws downstream of debris flow Sabo dams. *Appl Mech Mater* 170–173:2071–2076
- Pierson TC (2005) Hyperconcentrated flow—transitional process between water flow and debris flow. In: Jakob M, Hungr O (eds) *Debris-flow hazards and related phenomena*. Springer, Berlin, pp 159–202
- Scheidl C, Chiari M, Kaitna R, Müllegger M, Krawtschuk A, Zimmermann T, Proske D (2013) Analysing debris-flow impact models, based on a small scale modelling approach. *Surv Geophys* 34:121–140
- Scott KM, Vallance J, Pringle PT (1995) *Sedimentology, behavior, and hazards of debris flows at Mount Rainier*. USGS professional paper 1547, US Geological Survey
- Sharpe CFS (1938) *Landslides and related phenomena: a study of mass-movements of soil and rock*. Columbia University Press, New York
- Swanston DN, Swanson FJ (1976) Timber harvesting, mass erosion, and steep-land forest geomorphology in the Pacific Northwest. *Geomorphol Eng* 4:199–221
- Takahashi T (2014) *Debris flow: mechanics, prediction and countermeasures*. CRC, New York
- Thielicke W, Stamhuis E (2010) Time resolved digital particle image velocimetry tool for Matlab. This code can be downloadable at the following website: <http://PIVlab.blogspot.com>
- Watanabe M, Mizuyama T, Uehara S (1980) Review of debris flow countermeasure facilities. *Jpn Erosion Control Eng Soc* 115:40–45
- Wenbing H, Guoqiang O (2006) Efficiency of slit dam prevention against non-viscous debris flow. *Wuhan Univ J Nat Sci* 11:865–869. doi:10.1007/BF02830178
- Zollinger F (1985) Debris detention basins in the European Alps. International symposium on erosion, debris flow and disaster prevention, Tsukuba, Japan, pp 433–438

Electronic supplementary material The online version of this article (doi:10.1007/s10346-017-0853-4) contains supplementary material, which is available to authorized users.

#### S. Choi · T. Kwon (✉)

Department of Civil and Environmental Engineering,  
Korea Advanced Institute of Science and Technology (KAIST),  
Daejeon, South Korea  
e-mail: t.kwon@kaist.ac.kr

#### S. Choi

e-mail: newsk@kaist.ac.kr

#### J. Lee

Construction and Technology Research Department,  
Land and Housing Institute,  
Daejeon, South Korea  
e-mail: andrew4502@lh.or.kr